

Chapter 4

Dynamics of collapsing and exploding ^{85}Rb Bose-Einstein condensates

4.1 Introduction

This Chapter presents a description of our experiments with ^{85}Rb BEC in the attractive self-interaction regime, where the condensate may become unstable and undergo a “collapse” if the attraction is sufficiently strong. The first part of the Chapter provides some background information about BEC collapse physics, including our early experiments to study them. We move on to a detailed description of the response of the BEC when the sign of the scattering length is quickly switched from positive to negative. At the end of the Chapter, we compare our data to recent theoretical models for the collapse dynamics.

The ^{85}Rb BEC system is an ideal candidate for studying the collapse instability because of the condensate’s tunable interactions. By ramping the magnetic field, we can easily change the sign and magnitude of the scattering length (and interaction strength). As discussed in Chapter 2, the BEC self-interaction is repulsive when the scattering length is positive, and attractive when a is negative. The existence of the ^{85}Rb Feshbach resonance, which leads to a magnetic-field-dependent scattering length, allowed us to gain tremendous insight into the collapse physics.

Before our experiments in ^{85}Rb , condensates with attractive interactions had received only limited study in a ^7Li BEC system with fixed negative scattering length. The early ^7Li BEC studies [28] showed evidence for an instability, but the data did

not allow for stringent tests of theory. More recent experiments in ^7Li have focused on the collapse process in a high temperature condensate, where the BEC was continually replenished by a cold thermal cloud, leading to a sequence of growth and collapse cycles [29, 30]. In contrast, our ^{85}Rb BEC experiments were conducted with nearly thermal-atom-free condensates, and we took full advantage of our experimental control of the scattering length to extract more information about the collapse process.

4.1.1 Stability condition for BEC with $a < 0$

A stable, harmonically trapped condensate with negative scattering length has a maximum or critical allowed number of atoms, N_{crit} . When the number in the condensate exceeds the critical number, $N_{BEC} > N_{crit}$, the attractive self-interaction dominates the repulsive zero-point energy of the confined condensate wavefunction. The stability condition for the BEC is defined as

$$\frac{N_{crit}|a|}{a_{ho}} = k_{collapse}, \quad (4.1)$$

where $a_{ho} = \sqrt{\hbar/(m\bar{\omega})}$ is the mean harmonic oscillator length of the trap potential (with mean frequency $\bar{\omega} = \sqrt[3]{\omega_r^2\omega_z}$) and $k_{collapse}=0.55$ is a constant [31]. One can also view equation (4.1) as defining a critical value for the magnitude of the negative scattering length, a_{crit} , if the number of BEC atoms is assumed to be fixed. The stability condition expressed in equation (4.1) was determined by studying the ground state of the GP equation as a function of the product $N|a|$ [31, 32]. When this product exceeds the stability condition, then no stable solution can be found for the ground state. Thus, one expects an initially stable BEC that experiences a change in scattering length such that $(a_{init} > 0) \rightarrow (a_{final} < a_{crit})$ to become unstable and collapse in some fashion.

In our early experiments [33], we found that an initially stable BEC undergoes a dramatic ($\sim 50\%$) number loss some time after the scattering length is decreased below a critical value. Typically, we label this number loss as the BEC ‘‘collapse’’. By measuring

the critical number of atoms for collapse at several different values of negative scattering length, we verified the functional form of equation (4.1). We also determined the value of $k_{collapse}$, which was significantly lower than the prediction of existing theory [32]. However, our more recent high-precision measurement of the Feshbach resonance parameters (see Chapter 7) has allowed us to revise our previous estimate of $k_{collapse}$. The new value is completely consistent with theory [31].

The collapse of the condensates was an all-or-nothing process. We never observed partial collapses; a given BEC would either collapse at negative a or remain stable, depending on whether or not the number exceeded N_{crit} . We saw no evidence for a macroscopic quantum tunneling phenomenon in the collapse process, as some theory work had suggested (see Ref. [34] and references therein). In fact, collapse process turned out to be so reproducible that we could use it to precisely measure the magnetic field. We accomplished this by first measuring N_{crit} and a_{crit} and then using our knowledge of the variable scattering length due to the Feshbach resonance.

On a daily basis, we found the initial magnetic field using a fairly simple procedure. We first prepared a stable BEC at some initial value of B-field that corresponded to a positive scattering length. We then ramped the B-field to change the sign and magnitude of the scattering length to a negative value near a_{crit} . We observed the resulting BEC number and noted which final magnetic fields (final scattering lengths) caused large BEC number loss. After determining N_{crit} and a_{crit} in this way, we found the absolute magnetic field using equation (4.1) in combination with the known dependence of scattering length on magnetic field. We extrapolated from B_{crit} to B_{zero} , the field where the scattering length vanishes (corresponding to $N_{crit} = \infty$). The value of B_{zero} provided us with a useful calibration point.

Utilizing the BEC collapse to measure the magnetic field proved to be a rapid and precise technique. We repeated the experimental cycle with different B-field ramps until N_{crit} and a_{crit} were known. In a period of about one-half hour, we could determine

the initial magnetic field to a ~ 5 mG precision. Precise knowledge of B_{init} and a_{init} was quite useful for a variety of other experiments described in this thesis.

4.1.2 Overview of collapse dynamics

Although our early BEC experiments in the attractive self-interaction regime verified the stability condition and showed that condensate collapse involves number loss, our data actually raised more questions than they answered. For instance, we could not initially determine the fate of the atoms that left the BEC. We had other unanswered questions regarding the details of the number loss: how quickly were the atoms going away and what was setting the timescale of the collapse? Furthermore, what exactly happened to the BEC wavefunction during the collapse process?

At the time of our experiments, existing theories of BEC collapse [35, 36, 37] predicted that an unstable BEC would implode on itself. The contraction of the BEC would presumably take place on the time scale of a trap oscillation, and the density would sharply increase after $T_{rad}/4 \simeq 14$ ms, where T_{rad} is the radial trap period. As a result of the density growth, 3-body recombination losses were expected to cause a rapid depletion of the BEC, preventing the formation of a true singularity in the density of the atom cloud.

To explore the dynamics of the collapse process and check the validity of the proposed theoretical pictures, we took full advantage of the variable scattering length of ^{85}Rb condensates. We changed the sign of a and observed the time-dependent response of the BEC. We were quite surprised by the complexity of the BEC collapse. Various phenomena were observed — an initial gradual contraction was followed by a supernova-like explosion of hot atoms. At the end, a small remnant condensate was left behind in an excited oscillatory state, and much of the initial condensate had completely disappeared from view. In the rest of this chapter, we detail the prominent features of the collapse process as well as the methods used to study them.

4.2 Preparing and manipulating the condensate

The first stage in our experiment was to form a stable ^{85}Rb condensate[26]. A standard double magneto-optical trap (MOT) system[19] was used to collect a cold sample of ^{85}Rb atoms in a low-pressure chamber. Once sufficient atoms had accumulated in the low-pressure science MOT, the atoms were loaded into a cylindrically symmetric cigar-shaped magnetic trap with frequencies $\nu_{radial} = 17.5$ Hz and $\nu_{axial} = 6.8$ Hz. Radio-frequency evaporation was then used to cool the sample to ~ 3 nK to form pure condensates containing $>90\%$ of the sample atoms. The final stages of evaporation were performed at 162.3 G where the scattering length is positive and stable condensates of up to 20,000 atoms could be created. After evaporative cooling, the magnetic field was ramped adiabatically to 166 G, where the scattering length was near zero. This provided a well-defined initial condition — the BEC would shrink to approach the size and shape of the harmonic oscillator ground state (see section 3.5.4). We note that in a few cases, the initial scattering length was chosen to be significantly different from zero; this allowed us to vary the initial density of the condensates over a wide range.

We developed various different magnetic field ramps into useful tools for studying the BEC collapse dynamics. The B-field control allowed us to adjust the mean-field interactions within the BEC to a variety of values on time scales as short as 0.1 ms. The obvious manipulation was to jump to some value of $a < a_{crit}$ to trigger a collapse, but the tunability of a also greatly aided in imaging the sample. Usually the condensate size was below the resolution limit of our imaging system ($7\mu\text{m}$ FWHM). However, we could ramp the scattering length to large positive values and use the repulsive interatomic interactions to expand the BEC before imaging, thus obtaining information on the pre-expansion condensate shape and number. A typical $a(t)$ sequence is shown in Figure 4.1. We have used a variety of such sequences to explore many aspects of the collapse and enhance the visibility of particular components of the sample.

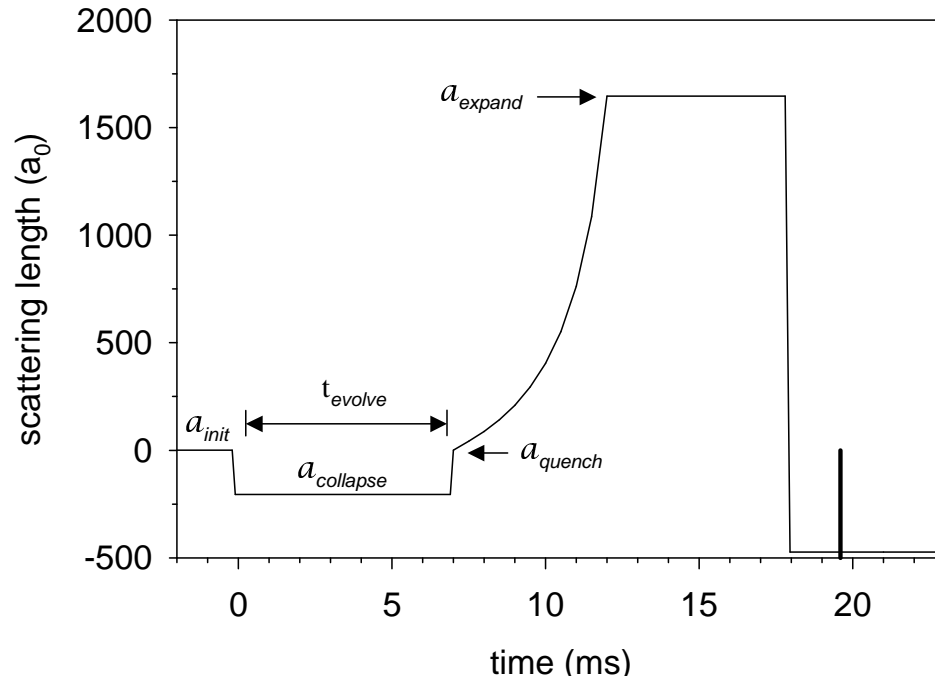


Figure 4.1: An example of experimental control of the scattering length. The thin solid line is the time dependent scattering length while the thick vertical line indicates the timing of the probe laser pulse for absorption imaging. We used a variety of $a(t)$ sequences similar to what is shown here to study the dynamics of the BEC collapse. To determine $a(t)$, we first calculated the magnetic field using a calibrated current sensor on the magnetic trap coil. Then we converted the B-field into scattering length using equation (2.2), the Feshbach theory expression for $a(B)$.

In Figure 4.1, the scattering length is jumped at $t = 0$ in 0.1 ms from $a_{init} \simeq 0$ to $a_{collapse} < 0$, where the BEC evolves for a time t_{evolve} . We carefully control the B-field so that magnetic field noise translates into fluctuations in $a_{collapse}$ on the order of $\sim 0.1 a_0$ in magnitude. After the time t_{evolve} , the BEC collapse process is then interrupted with a jump to a_{quench} , and the field is ramped in 5 ms to a large positive scattering length which makes the BEC expand. After 7.5 ms of additional expansion, the trap is turned off in 0.1 ms and 1.8 ms later the density distribution is probed using destructive absorption imaging with a $40 \mu\text{s}$ laser pulse (indicated by the vertical bar in Figure 4.1). In some instances, we increased the expansion time after the trap turn-off to further expand the BEC wavefunction.

As discussed in section 3.5.3, the increase in a from $a_{collapse}$ to a_{expand} is far too rapid to allow for the BEC to expand adiabatically. On the contrary, the smaller the BEC before expansion, the larger the cloud at the moment of imaging. Thus we can readily infer the relative size of the BEC wavefunction just prior to the jump to a_{quench} . After the mean-field expansion, the density of the expanded BEC is so low that the rapid transit of the Feshbach resonance [38] during the trap turn-off and the subsequent time spent at $B = 0$ ($a = -470 a_0$) both have a negligible effect.

4.3 BEC number loss

4.3.1 BEC number versus t_{evolve}

When the scattering length is jumped to a value $a_{collapse} < a_{crit}$, the BEC kinetic energy no longer provides a sufficient barrier against collapse. After making such a scattering length jump, we observed a delayed and abrupt onset of number loss from the condensate. As a function of the time spent at $a < 0$, the BEC number remained steady for a while, then dropped exponentially with a time constant τ_{decay} . This trend is illustrated by Figure 4.2, which is a plot of the condensate number N_{BEC} versus the

evolution time, t_{evolve} at a negative scattering length. Here the observed delay time before the onset of number loss is defined as the collapse time, $t_{collapse}$. The exponential number decay finally leveled off at a value N_{rem} , which we define as the remnant BEC number. N_{rem} was typically $\simeq 40\%$ of the initial number, N_{init} .

Although N_{BEC} was constant for a short time after the jump to $a_{collapse}$, we did observe some slight changes to the expanded condensate radius during t_{evolve} . These radius changes indicated that the BEC was contracting during the evolution time. Since the pre-expansion BEC was smaller than our resolution limit, we could not observe the contraction directly; however, we could infer the extent of the contraction by observing the degree of mean-field expansion. In fact, the BEC expanded more and more during the expansion ramp of Figure 4.1 as it contracted more and more during t_{evolve} . We actually observed that the post-expansion condensate widths changed very little with time t_{evolve} before $t_{collapse}$. For the data in Figure 4.2, the expanded radial BEC width increased by only 10% as t_{evolve} increased from 0 ms to 3.5 ms. The axial BEC width showed even less of a change.

From this we infer that the cloud of condensate atoms did not contract dramatically before loss began. To obtain a quantitative estimate for the amount of contraction, we use the equations in Ref. [27]. The PG model results provide a fairly good match to the observed expanded BEC shape over a moderate range of $a_{collapse}$ and time before collapse. We can therefore have some confidence in using the equations of Ref. [27] to estimate the density before collapse. Surprisingly, we find that the predicted contraction corresponds to only a 50% increase in the average density (to $2.7 \times 10^{13} \text{ cm}^{-3}$) before the beginning of the number loss. Using the inelastic collision rates for ^{85}Rb that we measured in Ref. [39], this density predicts a loss time that is far longer than what we observe ($\tau_{inelastic} \sim 2.5 \text{ s}$) and does not have the observed sudden onset. Thus, our simple estimates of the BEC contraction and inelastic loss do not jibe with the observed behavior in Figure 4.2. The disagreement implies that the conventional simple picture

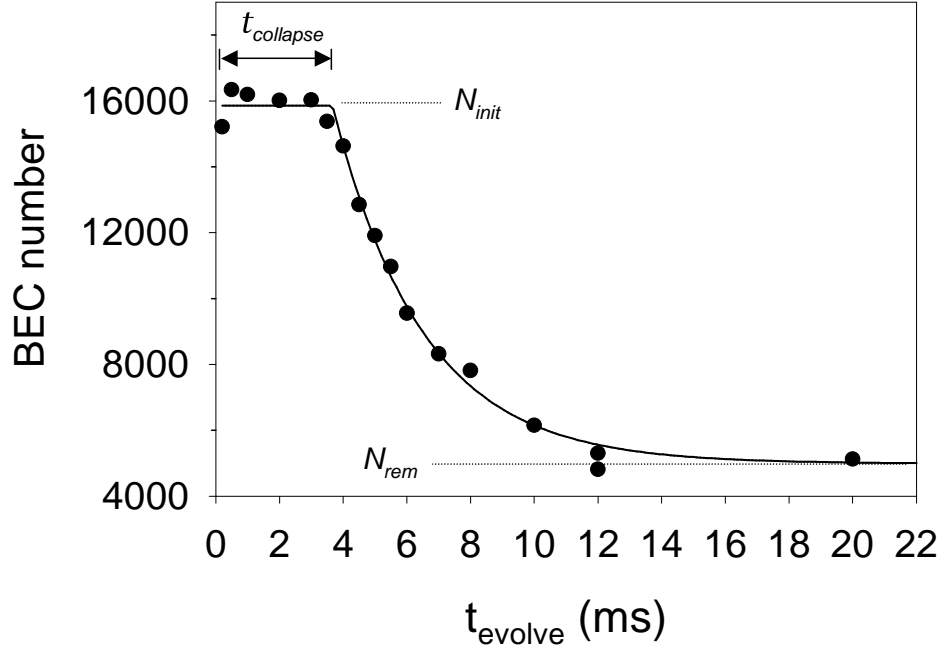


Figure 4.2: The condensate number versus time after a jump to a negative scattering length. Points are the number of atoms remaining in the BEC versus t_{evolve} at $a_{\text{collapse}} = -36 a_0$. The initial scattering length before the jump was $a_{\text{init}} = +8 a_0$ and the initial number of condensate atoms was $N_{\text{init}} = 16,000$. These conditions produced an estimated average initial density of $1.8 \times 10^{13}/\text{cm}^3$. We observed a delayed and abrupt onset of loss from the BEC number. The solid line is a fit to the data using a delayed exponential function with a best fit value of $t_{\text{collapse}} \simeq 3.7(5)$ ms for the delay. The number of atoms remaining in the condensate after the end of the decay process is $N_{\text{rem}} \sim 5000$.

of the collapse as a global implosion of the entire BEC wavefunction is incorrect. We will provide additional discussion of this point in section 4.5.3.

For the data in Figure 4.2 and most other data presented in this Chapter, we jumped to $a_{quench} = 0$ in 0.1 ms after a time t_{evolve} at $a_{collapse}$. We believe that the number loss stopped immediately after the jump. This interpretation is based on the surprising observation that the quantitative details of curves such as that shown in Figure 4.2 did not depend on whether the collapse was terminated by a jump to $a_{quench} = 0$ or $a_{quench} = 250 a_0$. Presumably, if there were a significant amount of loss occurring after the “quenching” ramp, then quantities such as N_{rem} and $t_{collapse}$ should depend on the precise value of a_{quench} ; however, this was not the case.

4.3.2 Variations in $t_{collapse}$

We have measured number decay curves like that in Figure 4.2 for many different values of the negative scattering length. The measured collapse time versus $|a_{collapse}|$ for fixed initial density is presented in Figure 4.3. As we increased $|a_{collapse}|$ from $7 a_0$ to $65 a_0$, the collapse time decreased by more than one order of magnitude. The data display a nearly perfect inverse dependence on the magnitude of the scattering length, as shown by the solid line.

We also studied the dependence of $t_{collapse}$ on the initial BEC density. By reducing N_{init} , we decreased the initial density from $\langle n_{init} \rangle = 2.8 \times 10^{13} \text{ cm}^{-3}$ to $\langle n_{init} \rangle = 1.1 \times 10^{13} \text{ cm}^{-3}$ (a factor of ~ 2.5). This change caused the collapse time to lengthen by a factor of 2.4(8) at $a_{collapse} = -8 a_0$. We verified that $t_{collapse}$ was truly proportional to density and not only to N_{init} by reducing the density through a volume change to the initial condensate. Holding N_{BEC} fixed at roughly 16,000 atoms, we decreased the initial density by a factor of 3.5 (with a corresponding increase in volume) by setting $a_{init} = +105 a_0$ instead of our more typical value, $a_{init} = +8 a_0$. At $a_{collapse} = -15 a_0$, the volume-induced density change caused $t_{collapse}$ to grow by roughly a factor of 3.

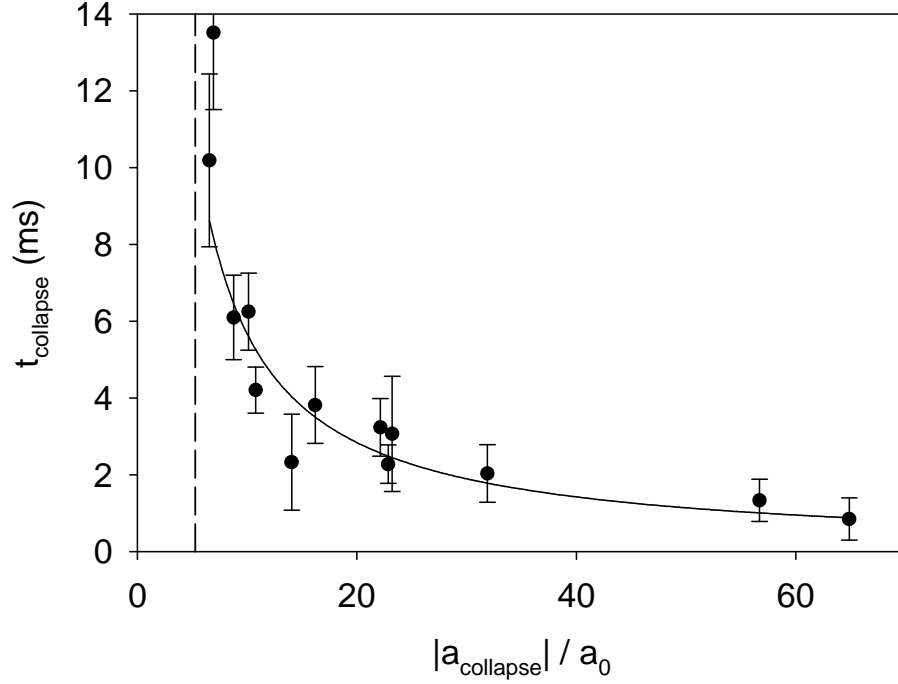


Figure 4.3: The collapse time versus $a_{collapse}$ for 6000 atom condensates. Points with error bars are the measured values of $t_{collapse}$. The solid line is a weighted fit to the function: $t = Q/a_{collapse}$, with $Q=57(6)$ ms a_0 . The vertical dashed line indicates a_{crit} for $N_0 = 6,000$. The data were acquired with $a_{init} = a_{quench} = 0(2)$ a_0 , so that the initial BEC density was $\langle n_{init} \rangle = 3(1) \times 10^{13}$ cm^{-3} . The average BEC densities given here were computed using the PG model (section 3.5.3) to determine the volume of the BEC wavefunction for a given value of the initial scattering length. We found that the PG model accurately predicts the mean density over the entire range of repulsive interactions, from the Thomas-Fermi limit of strong interactions to the non-interacting limit.

The observed dependences of the collapse time on scattering length and density indicate that there is some critical condition that must be reached before the onset of number loss. The time to reach the critical condition becomes smaller as we increase $\langle n_{init} \rangle$ and $|a_{collapse}|$. All of our evidence supports the idea that $t_{collapse}$ is inversely proportional to the magnitude of the attractive mean-field interaction: $E_{mf} \propto \langle n \rangle a$. This dependence seems reasonable since the rate of implosion of the BEC should depend on E_{mf} .

In contrast to $t_{collapse}$, the atom loss time constant τ_{decay} depended only weakly on $a_{collapse}$ and $\langle n_{init} \rangle$. For the range of $a_{collapse}$ shown in Figure 4.3, τ_{decay} did not depend on $a_{collapse}$ or $\langle n_{init} \rangle$ by more than the $\sim 20\%$ experimental noise in the τ_{decay} determination. On average, τ_{decay} was 2.8(1) ms. For the very negative value of $a_{collapse} \simeq -290 a_0$, however, τ_{decay} did decrease to 1.8 ms for $N_{init} = 6,000$ and 1.2 ms for $N_{init} = 15,000$.

4.4 Energetic burst of atoms

Thus far we have not explained what happens to the atoms after they exit the condensate during a collapse. As displayed in Figure 4.2, a large fraction of the atoms leave the BEC during the exponential decay. There are at least two components to the expelled atoms. One component (known as the “missing atoms”) is not detected in the absorption images. The other component emerges as a burst of detectable, spin-polarized atoms with energies much greater than the initial condensate’s energy but much less than the magnetic trap depth. The bizarre properties of the burst and its surprising formation during the BEC collapse prompted Carl Wieman and Eric Cornell to name it a “Bosenova”, in analogy with a supernova. In our attempts to understand the origins of the burst, we have studied the details of the burst atom distribution under a wide range of conditions. The average energy and number of the burst atoms depend in a complex manner on $a_{collapse}$ and N_{init} . Although the details are complicated, we present them here because they provide a stringent test of collapse theories.

The angular kinetic energy distribution with which the burst atoms are expelled from the condensate can most accurately be measured by observing the harmonic oscillations of the atoms in the trap, as illustrated in Figure 4.4(**a**). For example, one-half of a radial period after the expulsion ($T_{rad}/2$), all burst atoms return to their initial radial positions. At times significantly before or after this radial “focus”, the burst cloud is too dilute to be observed. Fortunately, at the radial focus, the oscillation trajectories along the axial trap axis are near their outer turning points. Therefore the axial energy can be found from the length of the stripe of atoms along the axial direction. The radial energy can be found with an identical procedure in an axial focus.

One can also define the “sharpness” of the burst focus as the minimum width in the narrow dimension. The harmonicity of the magnetic trap potential ensures that the sharpness of the burst focus should only depend on the duration of time that burst atoms are expelled from the BEC (the length of the explosion) and the initial spatial distribution of the atoms before the explosion. In principle we can therefore determine the formation time for the burst atoms by measuring the narrow width of the burst focus. However, this technique only allows us to set an upper limit on the burst creation time because of significant broadening of the images from our finite optical resolution limit. The upper limit from the burst focus sharpness is consistent with a direct measurement of the burst generation time (~ 1.2 ms) in section 4.4.1.

Figure 4.4(**b**) shows an image of a radial focus. The size scales for the burst focus and the remnant were always well separated since the latter was not expanded when we imaged the burst. Figure 4.4(**c**) shows axial cross sections of the image in part (**b**) and the fit cross sections for the burst and thermal clouds. The burst spatial distribution was well fit by a 2-D Gaussian function whose width in the long dimension corresponded to the average energy of the burst atoms.

Since the burst atom cloud extended far out into the edges of the absorption images and the optical depth was fairly low in the outer wings of the atom distribution,

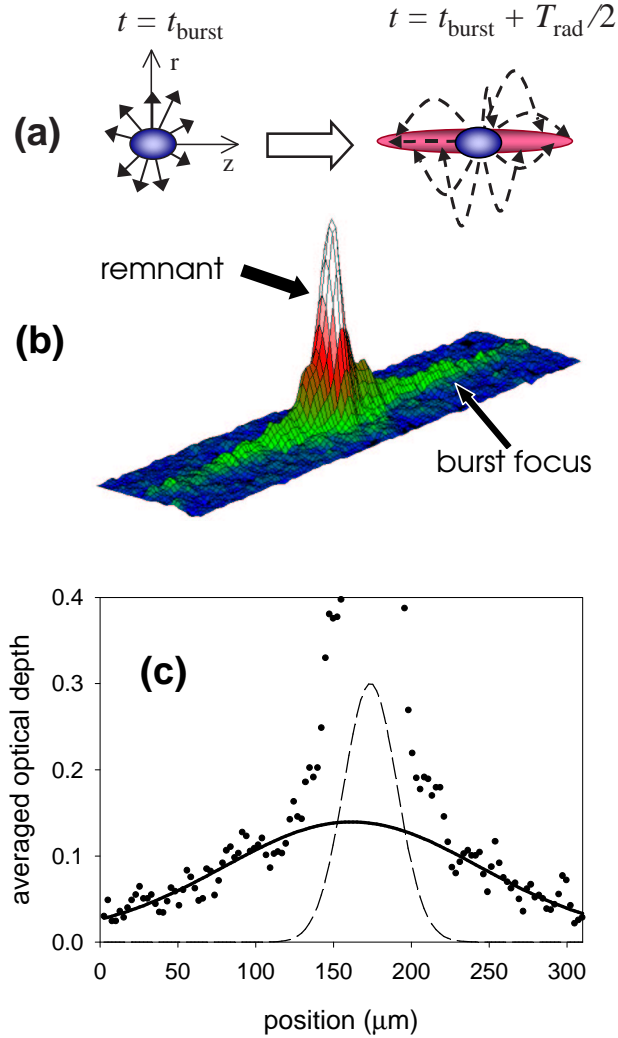


Figure 4.4: A burst focus. (a). Conceptual illustration of a radial burst focus. (b) An image of a radial burst focus taken 33.5 ms after a jump from $a_{\text{init}} = 0$ to $-36 a_0$ for $N_0 = 15,000$. Here $T_{\text{rad}}/2 = 28.6$ ms, which indicates that the burst occurred 4.9(5) ms after the jump. The average axial energy for this burst was $\langle E_{\text{burst},\text{axial}} \rangle = 62$ nK. The image dimensions are $60 \times 310 \mu\text{m}$. (c) Radially averaged cross section of the image in (b) along with a Gaussian fit to the burst spatial distribution. The central $100 \mu\text{m}$ were excluded from the fit to avoid fitting distortions from the condensate remnant and the thermal cloud. The rms widths of the BEC remnant and thermal cloud were $\sigma = 9 \mu\text{m}$ and $\sigma = 17 \mu\text{m}$, respectively. A small cloud of thermal atoms is present in the pre-collapse sample due to the finite temperature; these atoms appear to be unaffected by the collapse. The dashed line indicates the fit to this initial thermal component. There is a clear offset between the centers of the burst and the remnant. This offset varies from shot to shot by an amount comparable to the offset shown.

we utilized an image-processing tool to reduce background noise and improve the image signal-to-noise ratio. Much of the “noise” in the absorption images is actually due to interference fringes from the coherent probe laser beam. We could therefore improve the fitting procedure by removing the periodic stripes from the images. The removal was done by calculating the spatial Fourier transform of the optical depth data, then removing the probe laser stripes from the image, and finally transforming back to real space. In this way, we could obtain reliable measurements of the average burst atom energy along the radial and axial directions.

The average energy was generally different for the two trap directions. The burst energy fluctuated from shot to shot by up to a factor of 2 for a given $a_{collapse}$. This variation is far larger than the measurement uncertainty or the variation in initial number (both $\sim 10\%$), and its source is unknown. The burst energy and the dependences of $\langle E_{burst} \rangle$ on N_{init} and $a_{collapse}$ will be described in section 4.4.2.

4.4.1 N_{burst} versus t_{evolve}

One of the most interesting aspects of the burst behavior was the increase in N_{burst} during the collapse process. When we interrupted the BEC collapse with a jump back to $a_{quench} = 0$ (see section 4.3.1), we also interrupted the growth of the burst. The “interrupted” burst atoms still refocused after sitting at $a = 0$ for the requisite one-half of a trap period. We found the energy of the atoms in the interrupted bursts to be the same, but the number of atoms was smaller than in the uninterrupted case. By changing the time at which the collapse was interrupted we could measure the time dependence of the creation of burst atoms.

The increase in the burst number with t_{evolve} is illustrated in Figure 4.5. The number of burst atoms N_{burst} grows exponentially with a time constant of 1.2 ms, starting at $t_{evolve}=3.5$ ms and reaching an asymptotic final number of ~ 2500 atoms for all times ≥ 7 ms. N_{burst} also levels off at roughly the same time as the remnant BEC

number displayed in part **(b)** of the figure. Despite the observed large variations in the burst number, the average energy of the burst atoms (~ 85 nK) does not change significantly over the range of t_{evolve} shown in Figure 4.5.

The interrupted burst data clearly show that the growth of the burst with time at negative scattering length mirrors the decay of atoms from the condensate — the time dependences for these two processes are quite similar. However, by comparing parts **(a)** and **(b)** of Figure 4.5, one can see that the number of burst atoms is far smaller than the number of atoms leaving the BEC — there are at least $11000 - 2500 = 8500$ missing atoms. At present, the fate of the missing atoms has not been determined by experiment. The prevailing hypothesis is that the missing atoms are due to 3-body recombination into molecules, where the molecular binding energy is converted into kinetic energy that is shared by the collision partners. We discuss the scattering length dependence of the missing fraction of atoms in section 4.5.2.

Somewhat surprisingly, the number of atoms in the burst did not depend on the scattering length, $a_{collapse}$. Although N_{burst} varied randomly by $\sim 20\%$ as $|a_{collapse}|$ increased from nearly $0 a_0$ to $350 a_0$, on average the fraction of atoms going into the burst remained fixed at roughly 20% of the initial BEC number. Larger initial condensates produced larger bursts in direct proportion, so that the burst fraction remained constant as a function of N_{init} .

4.4.2 $\langle E_{burst} \rangle$ versus $a_{collapse}$

We carefully examined the scattering length dependence of the burst energy as one part of our collapse dynamics experiment. Although the burst energies were seen to vary from shot to shot, the average value for the energy was well defined and showed large-scale trends that dominated the shot-to-shot variations. We show the axial and radial burst energies versus $a_{collapse}$ in Figure 4.6**(a)** and 4.6**(b)** for $N_{init} = 6,000$ and 15,000, respectively.

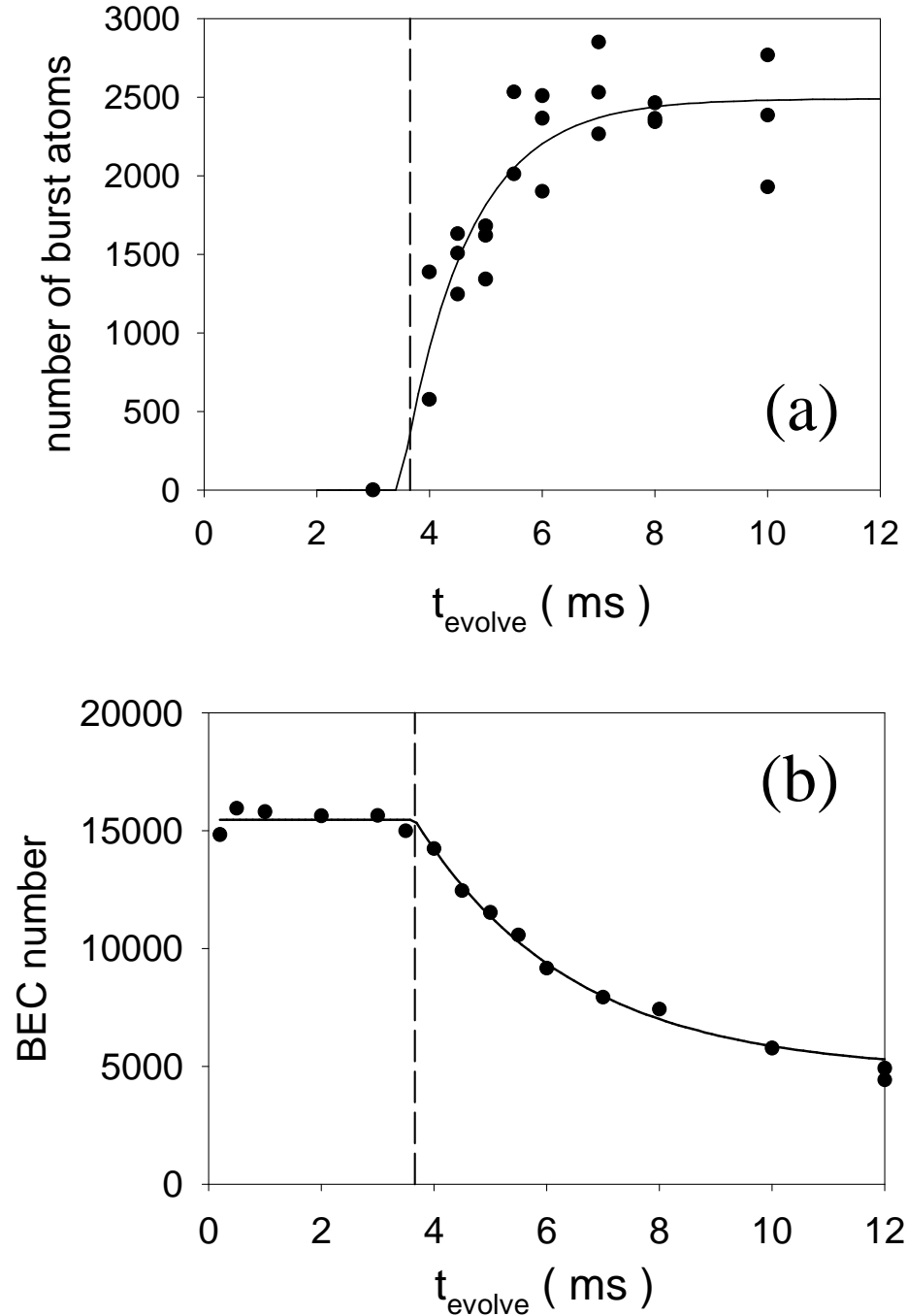


Figure 4.5: Growth of burst number with t_{evolve} . The data were collected under the same conditions as for Figure 4.2. (a) The points are N_{burst} versus evolution time at $a_{\text{collapse}} = -36 a_0$. The solid line shows the best fit of the data to a rising exponential function with time constant $\tau = 1.2(3)$ ms. The dashed vertical line indicates the best fit value for t_{collapse} from a fit to the BEC loss data in part (b). Figure (b) displays the BEC number decay for comparison to the burst growth data. The burst growth begins and ends at about the same time as the condensate loss. The time constants for BEC loss and burst growth are also comparable: $\tau_{\text{BEC}} = 2.7(3)$ and $\tau_{\text{burst}} = 1.2(3)$ ms.

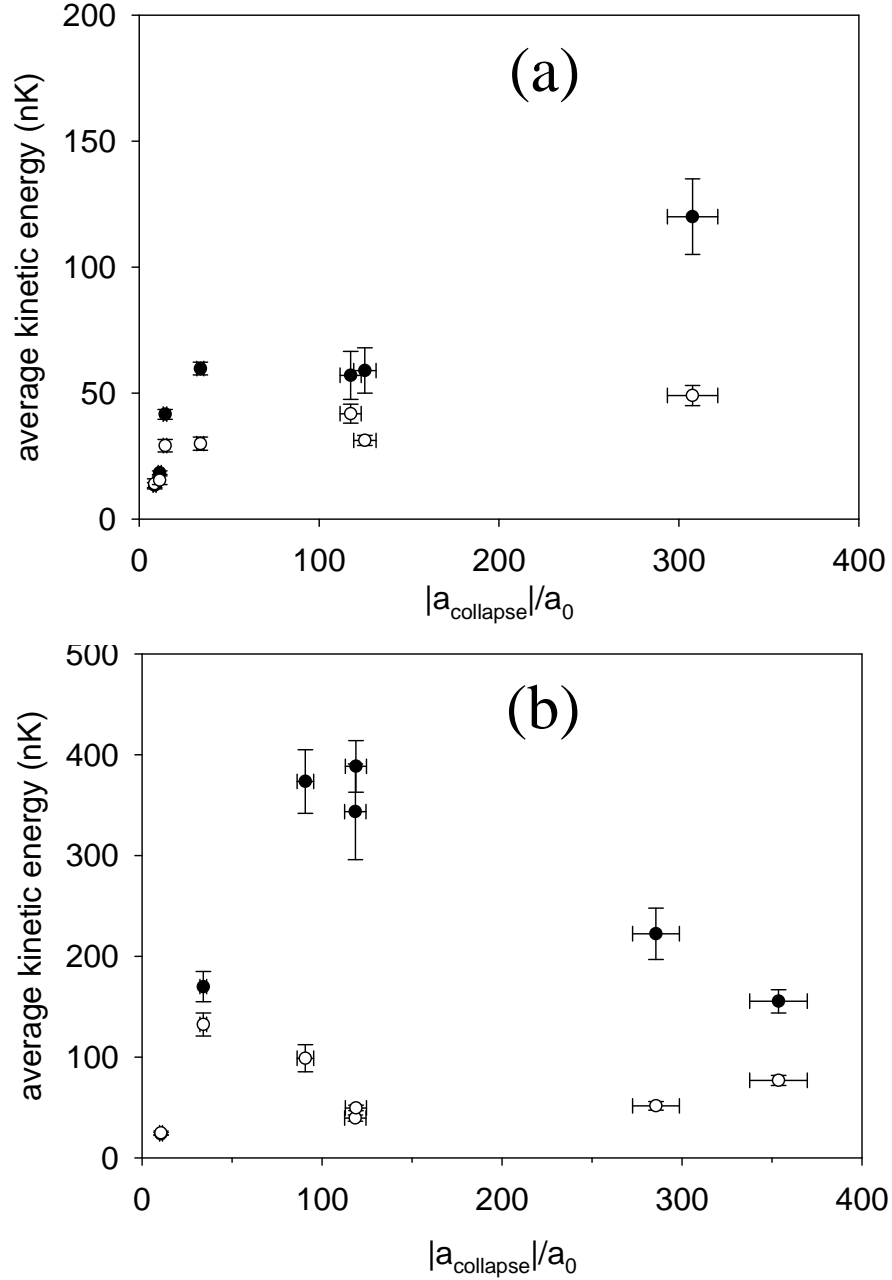


Figure 4.6: Average burst atom energy versus scattering length. (a) and (b) show the average axial and radial burst energies versus $|a_{collapse}|$ for $N_{init} \simeq 6,000$ and $N_{init} \simeq 15,000$, respectively. Filled points are the radial burst energies; open points are the axial energies. The average energy is calculated from the rms width, σ , of the 2-D Gaussian fit to the data as shown in Figure 4.4. For a given dimension, the average energy is $\langle E_{burst,i} \rangle = m\omega_i^2\sigma^2/2$, where ω_i is the trap frequency in the i^{th} dimension. On average, ten burst focuses were measured for each trap direction at each value of $a_{collapse}$ studied. The vertical and horizontal error bars indicate the standard error of the measurements and the uncertainty in $a_{collapse}$ arising from the magnetic-field calibration, respectively. For some of the points, the uncertainties are comparable to the symbol size.

The most striking feature of the data is the strong dependence of the average energy on the number of condensate atoms. Comparing **(a)** and **(b)**, one sees that for fixed $|a_{collapse}| \simeq 30 a_0$, the radial and axial burst energies increase by a factor of ~ 3 as the initial condensate number increases by $2.5\times$. In fact, the energies were higher for the larger N_{init} condensates over the full range of $a_{collapse}$ studied. An additional observation is the overall trend of increasing energy with increasing $|a_{collapse}|$ in the low N_{init} data (Figure 4.6**(a)**). However, the high N_{init} data in part **(b)** display much more complex behavior that is not monotonic with $a_{collapse}$.

We also note that over much of the scattering length range shown in Figure 4.6 there is a significant anisotropy in the burst energy. The radial energy is always greater than or equal to the axial energy. We discovered that the burst energy anisotropy depended on N_{init} , $a_{collapse}$, and a_{init} . The anisotropy showed a peaked behavior for 15000 atom condensates, with maximum near $|a_{collapse}| \sim 100 a_0$. For values of $|a_{collapse}|$ only slightly larger than $|a_{crit}|$, the burst was isotropic for both $N_{init} \simeq 6,000$ and $N_{init} \simeq 15,000$. At larger values of $|a_{collapse}|$, condensates with larger number gave rise to stronger anisotropies.

We cannot rule out a possible dependence of the burst energy anisotropy on the initial aspect ratio of the cloud, λ . We define λ as the ratio of the axial and radial rms widths of the BEC: $\lambda = \sigma_z/\sigma_r$. For the data with $N_{init} = 6000$, the initial scattering length was $a_{init} \simeq 0 a_0$, leading to $\lambda = 1.6$. In contrast, the high number data with $N_{init} = 15,000$ had $a_{init} \simeq +8 a_0$ and $\lambda = 2$. When instead we started at $a_{init} = +100 a_0$ ($N_{init}=15,000$), the BEC was initially more anisotropic ($\lambda = 2.4$), but the burst became more isotropic, with $\langle E_{ax} \rangle$ going up by $\sim 40\%$ and $\langle E_{rad} \rangle$ dropping by $\sim 60\%$ at $a_{collapse} = -100 a_0$. These various results for the burst energy and the energy anisotropy are clearly very complicated. It is impossible to say how much of the observed differences between the low number and high number data in Figure 4.6 are due to the change in N_{init} because we also changed the initial scattering length between

these two data sets. Nevertheless, the measured burst energy dependences can be used to test the validity of several mean-field models that were recently proposed to explain our results (see section 4.7).

4.5 Remnant BEC

4.5.1 N_{rem} exceeds N_{crit}

After each collapse, a “remnant” condensate containing a fraction of the atoms survived with nearly constant number for more than one second. The remnant BEC oscillated in a highly excited collective state with the two lowest breathing modes at $\nu \simeq 2\nu_{axial}$ and $\nu \simeq 2\nu_{radial}$ being predominantly excited. The measured frequencies were $\nu = 13.6(6)$ Hz and $\nu = 33.4(3)$ Hz. To find these oscillation frequencies, we measured the widths of the condensate as a function of the time spent at $a_{collapse}$. As usual, we utilized a mean-field expansion of the BEC to measure the widths. While the expansion leads to large increases in the widths, it does not distort their periodic modulation in time.

The number of atoms in the remnant depended on $a_{collapse}$ and N_{init} , and in general was not limited by the critical number, N_{crit} . Although the stability condition in equation (4.1) certainly determined whether or not the condensates experienced a collapse event [33], the number of atoms left behind was often significantly larger than N_{crit} . This behavior is shown in Figure 4.7, where we plot the remnant number as a function of scattering length.

In Figure 4.7, the 6000 atom data do mostly lie on or below the line showing the value of the critical number. In fact, for $N_{init} = 6,000$ and $|a_{collapse}| < 10 a_0$, more atoms were lost than the number required to lower N_{rem} below N_{crit} . Since we did not take the large N_{init} data until much later, we initially believed that N_{crit} truly did constrain $N_{remnant}$. However, the agreement observed in the $N_{init}=6000$ data

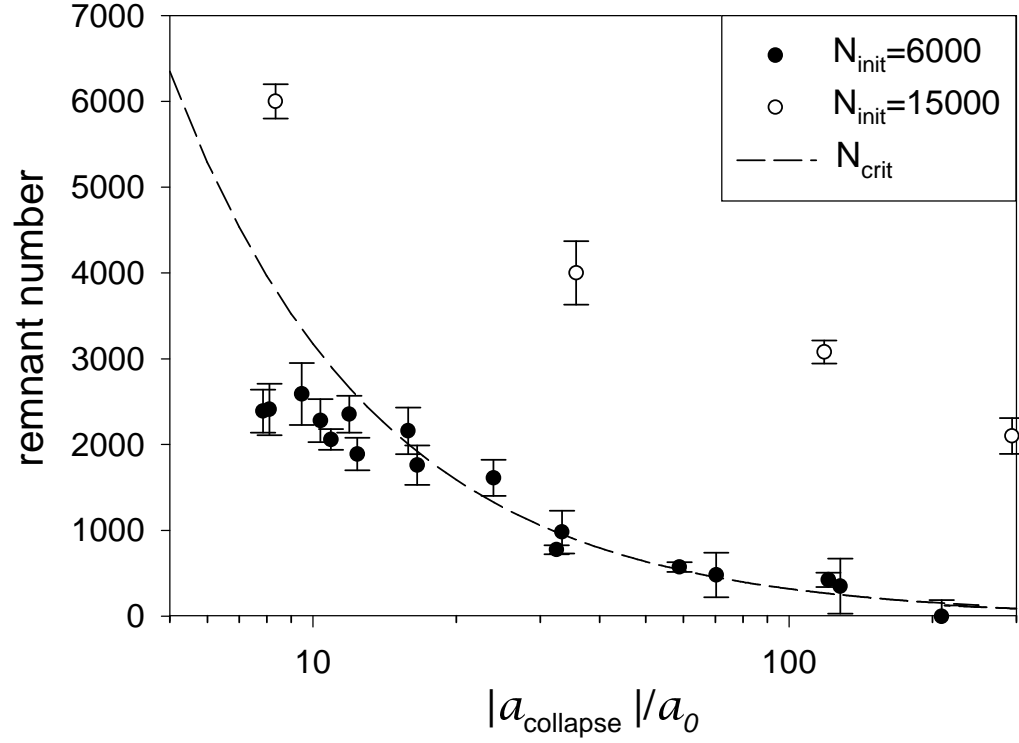


Figure 4.7: Remnant BEC number versus initial BEC number. The dashed line is the critical number of BEC atoms as calculated from the stability equation (4.1) with $k_{collapse}=0.55$ [31]. The black points and white points are the values of N_{rem} for different initial number, as explained in the legend. Note that the $N_{init}=6000$ remnant data (black points) correspond to the data we used for determining the collapse time as a function of scattering length in Figure 4.3.

turned out to be entirely coincidental; when we increased the initial number to $\sim 16,000$ atoms, the remnant number always exceeded N_{crit} for the entire range of $|a_{collapse}|$ that we investigated. The fraction of initial number of atoms that went into the remnant decreased with $|a_{collapse}|$, and was $\sim 40\%$ for $|a_{collapse}| < 10 a_0$ and $\sim 50\%$ for $|a_{collapse}| > 100 a_0$.

We found that a fixed fraction of N_{init} went into the BEC remnant independent of the value of N_{init} , so that smaller condensates often ended up with $N_{rem} < N_{cr}$, but larger condensates rarely did. After discovering this surprising result, we studied the remnant dependence on initial number in the condensate. Figure 4.8 demonstrates the direct proportionality between N_{rem} and N_{init} for fixed scattering length. Increasing the value of $|a_{collapse}|$ merely shifts the proportionality constant downward — the linear dependence remains.

The observation that the remnant number routinely exceeded the critical number is surprising, but not impossible to explain. One reason that we might expect this behavior is the highly excited state of the remnant. Due to the excitations and large number losses, it is difficult to know the proper temperature of the cloud. It is possible that the remnant is not actually a condensate, although the observed mean-field expansion of the atom cloud indicates that the phase space density is comparable to unity. Another possible explanation for N_{rem} exceeding N_{crit} is an inherent stabilizing nature of the excitations. Pattanayak et al. [40] have shown that a BEC with a particular type of collective excitation known as a quadrupolar shape oscillation can impart enough angular momentum the BEC to provide a centrifugal barrier to collapse. The excitation can stabilize a condensate by creating an additional quantum pressure beyond that provided by the confining trap potential. However, Ref. [40] also predicts that radial breathing mode excitations should *destabilize* a BEC with attractive interactions. Since we have observed breathing mode oscillations in the condensate widths, the Pattanayak et al. mechanism for stabilization is unlikely to explain our results. It would be inter-

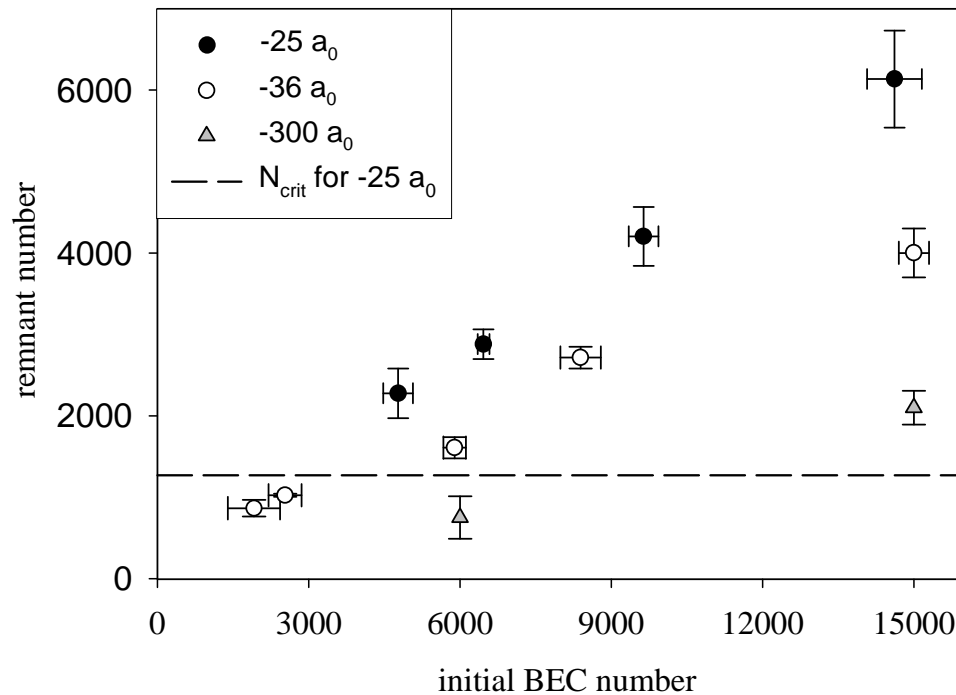


Figure 4.8: Dependence of remnant number on initial BEC number. The points are the measured values of N_{rem} versus N_{init} . The legend lists the various different values of $|a_{collapse}|$ that were used. The dashed line shows the critical number for the smallest relevant value of $|a_{collapse}|=25 a_0$. Most of the data clearly lie above this stability line. For the data with $|a_{collapse}|=25 a_0$, we found no discernible dependence of N_{rem} on initial scattering length when a_{init} was varied between $-1 a_0$ and $+6 a_0$.

esting to return to the issue of the BEC excitations and the apparent stabilization of the remnant in the future. One observable that might give useful information, but was not yet studied carefully is the excitation amplitude of the remnant cloud. Perhaps we could determine whether the oscillation amplitude is bigger for the collapse events in which N_{rem} greatly exceeds N_{crit} .

4.5.2 Missing atoms

In the collapse process, a large fraction of the initial BEC disappears. The missing atoms do not show up in the absorption images of the post-collapse BEC. Although we cannot yet say what happens to these expelled atoms, we are able to discuss the dependence of the missing atoms on scattering length and initial number because we know the corresponding trends for the burst and remnant numbers. Since N_{burst} was independent of $|a_{collapse}|$ but N_{rem} decreased with $|a_{collapse}|$, the number of missing atoms grew larger with $|a_{collapse}|$.

Interestingly, the absolute number of missing atoms also increased with N_{init} . The increase was proportional to the initial number so that the missing fraction dependence on $|a_{collapse}|$ was identical for both $N_{init} = 6,000$ and $N_{init} = 15,000$. For $|a_{collapse}| < 10 a_0$, we measured a missing fraction of $\sim 40\%$, while the fraction was $\sim 70\%$ for $|a_{collapse}| \geq 100 a_0$. The missing atoms were presumably either expelled from the condensate at such high energies that we could not detect them ($> 1 \mu\text{K}$), or they were transferred to untrapped atomic states or undetectable molecular states.

We made an attempt to test the hot atom hypothesis for the missing atoms by turning off the magnetic trap immediately after a collapse and then recapturing the atoms in the MOT. Because the MOT trap depth of order $\sim 1 \text{ K}$ is much deeper than that of the magnetic trap ($\sim 100 \mu\text{K}$), the recapture process should collect atoms with much higher energy than we could ever observe with absorption imaging. An additional advantage of the MOT is its large trap volume, which greatly exceeds the magnetic

trap volume. However, recapture in a MOT and subsequent fluorescence detection suffers from two major defects that we could not surmount. The first defect is the poor sensitivity of fluorescence detection versus absorption imaging. For small atom samples, there simply is not much light scattered by the atoms for detection. The sensitivity problem can be solved by careful design of a high-gain photodiode circuit. However, there is another problem with the MOT recapture, namely, the large background signal due to hot “Oort cloud” atoms in the magnetic trap. The Oort cloud is thought to form during the evaporative cooling process and to interact only very weakly (if at all) with the BEC [41]. In fluorescence detection, the Oort cloud atom signal swamps the BEC signal due to a difference in the numbers of atoms of many orders of magnitude. As a result, we could not make a quantitative search for the missing atoms with the magneto-optical trap.

4.5.3 Strange density patterns: jets

Under certain experimental conditions, we observed streams of atoms with highly anisotropic velocity distributions emerging from the collapsing condensates. Atoms in the “jets” possess distinctly different properties from the burst atoms. First, the jets have much lower kinetic energy than the burst (a few nK compared to ~ 100 nK). The average velocity of the jet atoms is nearly purely radial, so that the energy anisotropy is at least 10. In addition, we have discovered that the jets appear only when the BEC collapse process is interrupted (i.e., by jumping to $a_{quench} = 0$) during the period of BEC number loss. When the collapsing condensate was allowed to complete the collapse process so that $N_{BEC} \rightarrow N_{rem}$, no jets were emitted from the BEC. In contrast to this behavior, the burst atom explosion always seemed spontaneous; bursts would form whether or not we quenched the collapse by quickly ramping to zero scattering length.

Examples of the strange jet density patterns we have observed are shown in

Figure 4.9 for different values of t_{evolve} and the same conditions as Figure 4.2. We observed that the jet size and shape varied from image to image even when all conditions were unchanged, and as many as three jets were occasionally emitted from the collapse of a single condensate. Surprisingly, the jets were not always symmetric about the condensate axis. We even observed that some jets were emitted at a slight angle with respect to the radial direction.

We hypothesize that the jets are manifestations of local “spikes” in the condensate density that grow while the BEC is imploding and then expand when the balance of forces is changed by quenching the collapse. If this interpretation is correct, we can estimate the size of the density spikes using the uncertainty principle. After a jump to $a_{quench} = 0$, the kinetic energy of the atoms in the resulting jet must be equal to the confinement energy that the spike had prior to quenching the collapse. If we assume a Gaussian density spike in the BEC wavefunction with a width σ , then the average kinetic energy of the jet atoms is related to the width of the spike by

$$\langle T \rangle = \frac{1}{2}m\langle v \rangle^2 = \frac{\hbar^2}{4m\sigma^2}. \quad (4.2)$$

In the context of the spike picture, the observed anisotropy of the jets indicates that the spikes from which they originated were also highly anisotropic, being narrower in the radial direction. From the calculated widths (using equation (4.2)) and the measured number of atoms in the jets, we can estimate the density in the spikes. We present plots of the number of jet atoms and the inferred spike density versus t_{evolve} in Figure 4.10. The jet data exhibited variability in energy and number significantly larger than the $\sim 10\%$ measurement noise.

The jets expanded with velocity $v \simeq 1$ mm/s, which corresponds to a kinetic energy of ~ 5 nK and a radial pre-quench Gaussian rms width of ~ 0.5 μm . Since the axial size of the jets was below our optical resolution limit, we could not measure the axial

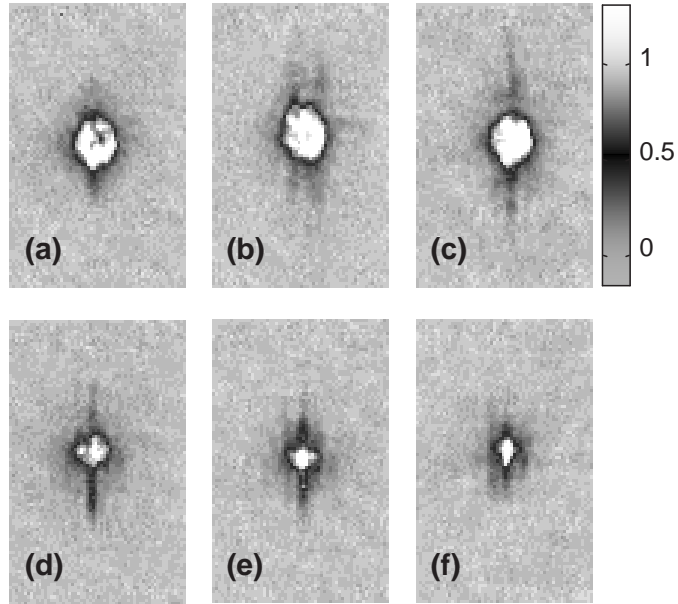


Figure 4.9: Jet images for a series of t_{evolve} values. The absorption images were taken with the conditions of Figure 4.2. The evolution times were 2, 3, 4, 6, 8, and 10 ms (from **(a)** to **(f)**). Each image has dimensions $150 \times 255 \mu\text{m}$. The shaded bar indicates the optical depth scale. For these data, we applied an expansion ramp to $a_{expand} = +250 a_0$, so the jets are longer than for the quantitative measurements explained in the text. The jets were longest (i.e., most energetic) and contained the most atoms at values of t_{evolve} for which the slope of the number loss curve (Figure 4.2) was greatest. A tiny jet is barely visible for $t_{evolve} \simeq 2$ ms (image **(a)**), which is 1.7 ms before $t_{collapse}$. The central component of the images is the remnant BEC, which clearly decreases with time. The time between the application of a_{quench} and the acquisition of the images was fixed at 5.2 ms.

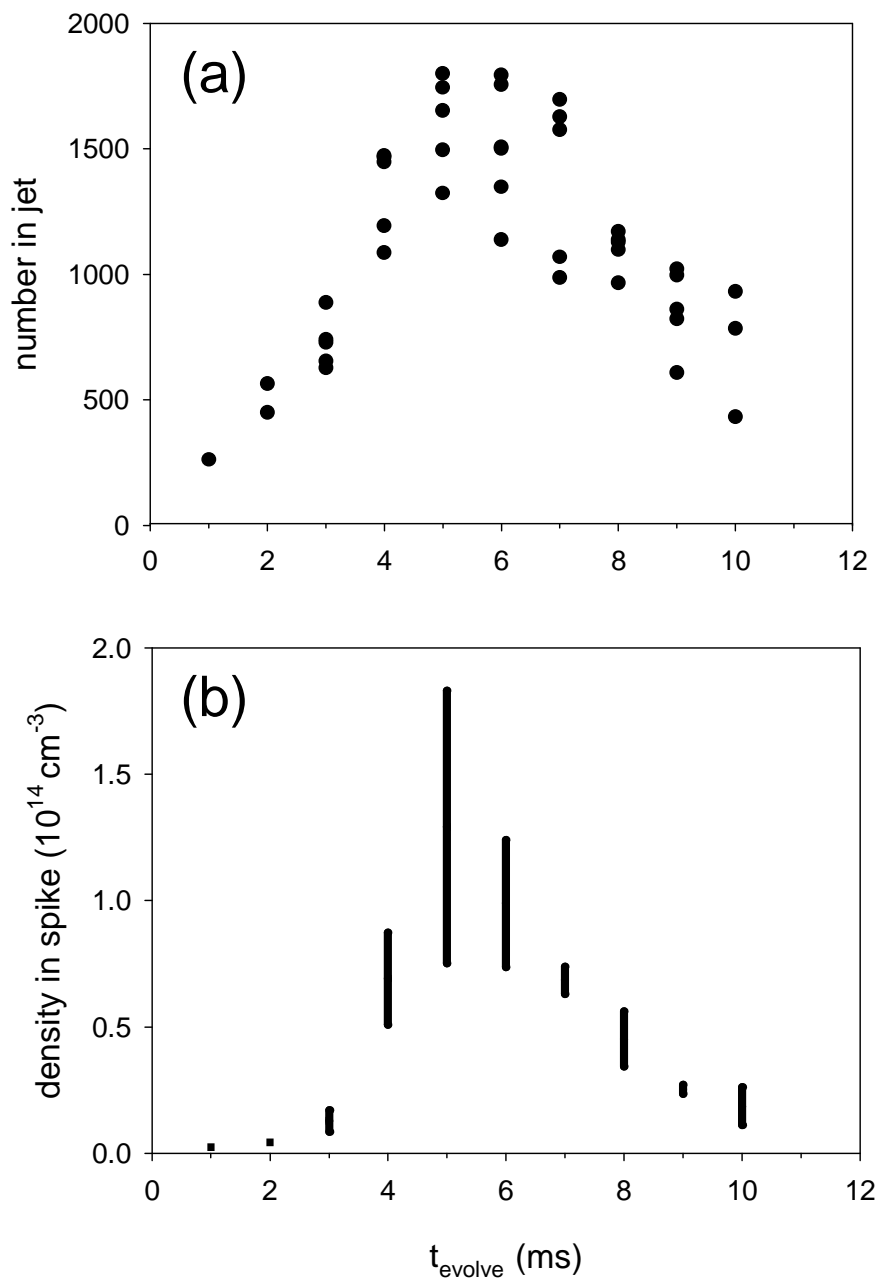


Figure 4.10: Quantitative jet measurements. (a) The number of atoms in the jets versus t_{evolve} for the conditions of Figure 4.2. (b) The spike density inferred from the kinetic energies of the jets. The vertical bars indicate the full range of shot-to-shot variability, which was rather high. For the analysis, we assumed the jets were disk-shaped since the magnetic trap has cylindrical symmetry. The images were taken perpendicular to the axial trap axis, corresponding to an edge-on view of the disks.

expansion rate. We therefore assumed an axial width equal to the harmonic oscillator length for estimating the spike density. The atom density in the spikes decreased for larger values of $|a_{collapse}|$, and was half as large for $a_{collapse} = -170 a_0$ as for $-36 a_0$.

The observation of jets in the collapsing condensates suggests that the collapse process involves a clumping of atoms into bunches. The implosion of the BEC probably cannot be simply characterized as an overall contraction with a single density peak at the center of the cloud [37]. In fact, we have evidence from mean-field expansion of the collapsing condensates (see section 4.3.1) that the overall density contraction is relatively small — with an average density increase on the order of 50%. So a more plausible picture of the collapse is one with internal structure, as suggested by more recent theoretical models. A discussion of the recent theory is given in section 4.7.

4.6 Collapse at B=0

In addition to the measurements described in this Chapter, it is potentially very interesting to examine the collapse of an ^{85}Rb BEC after turning off the magnetic trap. When the trap potential is switched off, we have the novel situation that the scattering length is large and negative ($\sim -470 a_0$ at B=0). We have not extensively studied the collapse dynamics at B=0 because most of the special techniques we have developed, such as mean-field expansion of the BEC and focusing the burst atoms, do not work at zero field.

However, when we quickly turn off the magnetic trap after forming a high density condensate, we do observe a burst of energetic atoms emerging from the BEC. At the same time, the number of condensate atoms decreases rapidly. Unfortunately, it is somewhat difficult to determine how much of the burst and number loss is due to collapse physics and how much is due to ramping the B-field across the Feshbach resonance (see Chapter 5). Nevertheless, the BEC collapse at B=0, and also at magnetic fields slightly below the Feshbach resonance, may provide an interesting avenue for future research.

4.7 Discussion of theoretical models

4.7.1 Overview of observations

Collapsing ^{85}Rb condensates display very dramatic and complex behavior. At the time that the data were collected, most of the observed details of the collapse could not be easily explained in terms of existing theoretical models for the collapse [36, 37, 42, 43, 44]. These theories were developed to describe ^7Li experiments, where the scattering length was fixed and the BEC interactions with a large thermal cloud proved very important. The peculiar and complex collapse behavior seen in our ^{85}Rb experiment prompted a number of theorists [45, 46, 47, 48] to adapt their models to our experimental conditions. To facilitate comparison of the prominent features of our data with the predictions of the theories, we can summarize our main observations.

- (1) There is a delayed and abrupt onset of number loss from the condensate after $a \rightarrow a_{collapse}$.
- (2) The delay time before the loss depends inversely on both the initial density and $|a_{collapse}|$.
- (3) The loss decay constant τ_{decay} is independent of both N_{init} and $|a_{collapse}|$ for $|a_{collapse}| < 100 a_0$, and only weakly depends on these quantities for larger $|a_{collapse}|$.
- (4) Part of the BEC number loss is due to formation of an energetic burst of atoms. The average burst energy and energy anisotropy exhibit dramatic variations with initial condensate number and $|a_{collapse}|$.
- (5) The number of cold remnant BEC atoms surviving the violent collapse varies between much less and much more than N_{crit} , depending on N_{init} and $a_{collapse}$.

4.7.2 Mean-field models for collapse

All of the papers that model the collapse dynamics experiments described in this Chapter [46, 47, 48] use a mean-field approach that includes density-dependent decay from the BEC. To account for 3-body recombination losses and also describe the attractive self-interaction in the BEC, the authors of Refs. [46, 47, 48] integrate a modified Gross-Pitaevskii (GP) equation that possesses an imaginary loss term [37].

Santos and Shlyapnikov [46] numerically integrate the modified GP equation for our anisotropic magnetic trap potential, using a particular value for the 3-body recombination loss coefficient, L_3 . The authors choose L_3 to be within the limits set by our previous experiments [39], with a typical choice being $L_3 = 2 \times 10^{-26} \text{ cm}^6/\text{s}$. The model of Ref. [46] shows that 3-body recombination losses set an upper to the contraction of the collapsing BEC. The density should grow until the loss “burns” a small number of atoms in the dense central region, then the region is quickly refilled by surrounding atoms. Santos and Shlyapnikov observe a series of such intermittent collapses of the BEC, with each collapse destroying only a small number of the condensate atoms. As the number decreases due to the losses, the balance of forces controlling the condensate wavefunction changes. The attractive mean-field interaction becomes weaker and is overcome by a repulsive force from the tight compression of the BEC wavefunction. Thus, each intermittent collapse has a compression phase followed by a rapid expansion or explosion of BEC atoms.

The authors of Ref. [46] therefore identify the burst atoms observed in the experiment as excited condensate atoms produced during the intermittent collapses. Obviously then, the missing atoms are the atoms that are burned off by 3-body recombination. Santos and Shlyapnikov make quantitative predictions for several experimental quantities, including $t_{collapse}$, τ_{decay} , and $\langle E_{burst} \rangle$ in the axial and radial directions. The model reproduces several of the prominent features of the experimental data, including the

BEC loss characteristics (features (1)-(3) above) and the observed fact (5) that N_{rem} is often much greater than N_{crit} . There is no explanation given for $N_{rem} > N_{crit}$ in the model — the authors simply state that this is “expected”!

Santos and Shlyapnikov assert that the energetically expanding BEC atoms are the burst atoms. The calculated burst energies are predicted to scale with the ratio $a_{collapse}^2/L_3$. By allowing L_3 to vary with scattering length from $\sim 2 \times 10^{-27}$ cm⁶/s at $a \simeq -30 a_0$ to $\sim 2 \times 10^{-25}$ cm⁶/s at $a \simeq -250 a_0$, Santos and Shlyapnikov obtain good agreement with the experimental data for $\langle E_{burst} \rangle$ with $N_{init}=6000$ atoms. However, the agreement with the larger $N_{init}=15,000$ data is quite poor. Overall then, Santos and Shlyapnikov cannot model the full experimental burst behavior (feature (4) above), even when they allow the loss rate coefficient to vary by a factor of 100. While Ref. [46] has intuitive appeal and does qualitatively explain all of the observations, it is impossible to fully evaluate the validity of the theory without better knowledge of the 3-body decay rates in the negative scattering length regime.

Other theoretical models have been developed to explain the collapse dynamics [47, 48]. Most notably, Saito and Ueda [47] have proposed a mean-field model that is nearly identical to that of Ref. [46], with the only quantitative difference being a smaller choice for the 3-body decay rate coefficient ($L_3 = 2 \times 10^{-28}$ cm⁶/s). Saito and Ueda also predict details of the BEC loss that agree with experiment and they observe a burst of energetic atoms. However, the authors make no attempt to model the burst energy because of the unknown L_3 dependence on scattering length. One unique prediction from Saito and Ueda regards the jets. The authors explain that the jets do not result from the released confinement energy of density spikes but instead are due to interference of matter waves emanating from different density clumps in the imploding BEC.

4.7.3 Beyond mean-field theory

Although the published theoretical models for the ^{85}Rb BEC collapse behavior are all based on conventional BEC mean-field theory, it is possible that the physics might require more complicated theories that go beyond the level of the GP equation. Murray Holland has expressed the opinion that the ^{85}Rb collapse is special because of the Feshbach resonance. He suggests that a quantum field theory that includes higher-order correlations between the atoms is necessary to fully explain our observations. In addition, T. Kohler and K. Burnett have also been pursuing a beyond-GP-equation approach to explain the burst atoms we observed during the collapse process (Ref. [46] contains a note about this). It will be interesting to see whether a full theory of resonant BEC can be developed to explain both the collapse experiments and the atom-molecule coherence experiments in Chapter 6.

On a related note, Jake Roberts has proposed an interesting experiment to study the collapse by changing the scattering length in a different way. We could use an RF π pulse to change the spin state of the atoms from $|2, -2\rangle$ to $|2, -1\rangle$. This state has a large negative scattering length and no nearby Feshbach resonance. Thus, by studying the collapse dynamics (especially the possible presence of burst atoms), one could potentially separate the physics of the collapse at fixed scattering length from the physics of resonant BEC.